

Higher-order topological electric circuits and topological corner resonance on the breathing Kagome and pyrochlore lattices

Motohiko Ezawa

Department of Applied Physics, University of Tokyo, Hongo 7-3-1, 113-8656, Japan

Electric circuits are known to realize topological quadrupole insulators. We explore electric circuits made of capacitors and inductors forming the breathing Kagome and pyrochlore lattices. They are known to possess three phases (trivial insulator, higher-order topological insulator and metallic phases) in the tight-binding model, where the topological phase is characterized by the emergence of zero-energy corner states. A topological phase transition is induced by tuning continuously the capacitance, which is possible by using variable capacitors. It is found that the two-point impedance yields huge resonance peaks when one node is taken at a corner in the topological phase. It is a good signal to detect a topological phase transition. We also show that the topological corner resonance is robust against randomness of capacitance and inductance. Furthermore, the size of electric circuits can be quite small to realize the topological phase together with topological phase transitions.

Introduction: Topological insulators and its generalization to higher-order topological insulators¹⁻¹² are fascinating topics in condensed-matter physics (CMP). They are characterized by the bulk symmetry and the bulk topological numbers, and observed by the emergence of topological zero-energy boundary states. Especially, topological zero-energy corner states emerge for the second-order topological insulators (SOTI) in two dimensions and for the third-order topological insulators in three dimensions. They are robust against impurities. They are studied mainly in fermionic systems in materials¹³⁻¹⁵. Actually, it is quite difficult to make experimental observation of topological corner states in CMP. Furthermore, although topological phase transitions have been extensively studied, the experimental observation is also very difficult in CMP. On the other hand, these topological corner states have already been observed experimentally in phononic system¹⁶⁻¹⁸, microwave system¹⁹, photonic system²⁰ and electric circuits²¹.

Topological corner states in square lattice are experimentally realized in electric circuits^{21,22}. Indeed, the Su-Schrieffer-Heeger model^{23,24}, the honeycomb lattice^{23,24} and Weyl semimetals^{23,25} have already been implemented in electric circuits. The impedance is a measurable quantity determining whether the system is topological or not, where topological boundary resonance effects occur in the topological phases. Here we note that the emergence of topological corner states has been predicted¹⁰ also in the breathing Kagome and pyrochlore lattices in the context of CMP. Thus, it is an interesting problem to study measurable quantities in topological electric circuits corresponding to these lattices.

Let us explain how to construct a topological electric circuit by taking an instance of the breathing Kagome lattice. The breathing Kagome lattice consists of lattice sites and two types of links indicated in red and cyan as in Fig.1(c). We insert capacitors with capacitance C_A and C_B to links in red and cyan, respectively, as in Fig.1(a). Then, we connect each lattice site to the ground via an inductor with inductance L , as illustrated in Fig.1(b). A lattice site is called a node in electric circuit. It is clear that this method is applicable to any lattices we encounter in CMP.

In this paper, we study electric circuits corresponding to the breathing Kagome and pyrochlore lattices. Topological phase

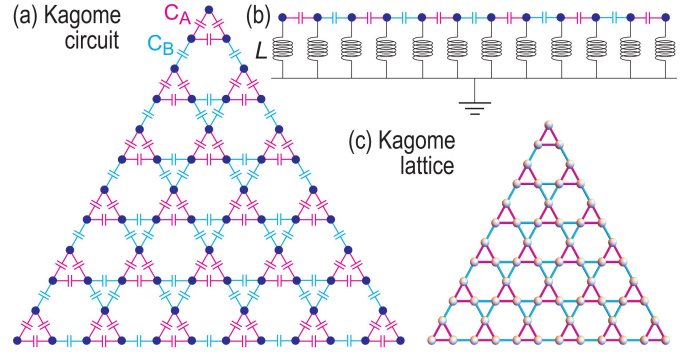


FIG. 1: Illustration of the breathing Kagome circuit composed of two types of capacitors (with capacitance C_A and C_B) and inductors (with inductance L). Adjacent nodes are connected by capacitors and each node is grounded by an inductor. The size of the triangle is $\ell = 6$.

transitions in electric circuits are well signaled by measuring the impedance, where huge resonance peaks emerge at corners in the topological phase. We find the topological robustness, that is, this resonance is robust against randomness of capacitance and inductance. We explicitly investigate a triangular geometry made of the breathing Kagome circuit, where we define its size ℓ by the number of small upper triangles along one edge: See Fig.1. We also study a tetrahedron geometry made of the breathing pyrochlore circuit.

Topological electric circuits: Electric circuits are characterized by the Kirchhoff's current law^{21,23,24},

$$\frac{d}{dt}I_a = \sum_b C_{ab} \frac{d^2}{dt^2} (V_a - V_b) + \frac{1}{L_a} V_a, \quad (1)$$

where I_a is the current between node a and the ground, V_a is the voltage at node a , C_{ab} is the capacitance between nodes a and b , $1/L_a$ is the inverse of the inductance at node a , and the sum is taken over all adjacent nodes b . See an example of the breathing Kagome circuit in Fig.1. When we apply an AC field $V(t) = V(0)e^{i\omega t}$, the Kirchhoff's law is rewritten as

$$I_a(\omega) = \sum_b J_{ab}(\omega) V_b(\omega) \quad (2)$$

with

$$J_{ab}(\omega) = i\omega \left[C_{ab} + \delta_{ab} \left(\sum_c C_{ac} - \frac{1}{\omega^2 L_a} \right) \right], \quad (3)$$

where the matrix $\mathbf{J}(\omega) = \{J_{ab}(\omega)\}$ is called the circuit Laplacian. It is a linear operator and corresponds to a tight-binding Hamiltonian H in CMP via the relation $J_{ab}(\omega) = i\omega H_{ab}(\omega)$ with the Hamiltonian being^{21,23}

$$H_{ab}(\omega) = C_{ab} + \delta_{ab} \left(\sum_c C_{ac} - \frac{1}{\omega^2 L_a} \right). \quad (4)$$

The capacitor between adjacent nodes a and b corresponds to the transfer integral $t_{ab} \leftrightarrow C_{ab}$ between adjacent sites a and b , while the inductor attached to node a corresponds to the on-site potential $U_a \leftrightarrow \sum_b C_{ab} - (1/\omega^2 L_a)$ at the site a . Later we present an explicit correspondence in the case of the breathing Kagome lattice.

By diagonalizing the matrix $\mathbf{J}(\omega)$ we obtain the eigenvalue j_n and the associated eigenmode $|\psi_n\rangle$. Then, we have $\mathbf{J}(\omega) = \sum_n j_n |\psi_n\rangle \langle \psi_n|$. The eigenmode $|\psi_n\rangle$ is a vector whose components are labelled by node a ; $|\psi_n\rangle = \{\psi_{n,a}\}$. The admittance eigenvalue j_n is a measurable quantity²⁴.

The two-point impedance is given by^{21,23}

$$Z_{ab} = \frac{V_a - V_b}{I_{ab}} = \sum_n \frac{|\psi_{n,a} - \psi_{n,b}|^2}{j_n}, \quad (5)$$

and determined by measuring the voltage response by running a current between two nodes a and b . The key property is that Z_{ab} diverges in the presence of zero-admittance modes ($j_n = 0$) provided $\psi_{n,a} \neq \psi_{n,b}$. Hence, the emergence of zero-admittance modes may be detected by measuring the two-point impedance.

Breathing Kagome circuit: The electric circuits corresponding to the honeycomb lattice have already been studied^{23,24}. Here we investigate them for the breathing Kagome lattice, which is known to realize a SOTI in CMP. We consider an infinite circuit which is periodic with a unit cell. It corresponds to a bulk system in CMP.

The circuit Laplacian (3) for an infinite circuit reads

$$J = i\omega \left[2(C_A + C_B) - \frac{1}{\omega^2 L} \right] \mathbb{I} - i\omega H_{\text{Kagome}}, \quad (6)$$

where \mathbb{I} is the unit matrix and

$$H_{\text{Kagome}} = \begin{pmatrix} 0 & h_{12} & h_{13} \\ h_{12}^* & 0 & h_{23} \\ h_{13}^* & h_{23}^* & 0 \end{pmatrix}, \quad (7)$$

with

$$\begin{aligned} h_{12} &= C_A + C_B e^{-i(k_x/2 + \sqrt{3}k_y/2)}, \\ h_{13} &= C_A + C_B e^{-ik_x}, \\ h_{23} &= C_A + C_B e^{i(-k_x/2 + \sqrt{3}k_y/2)}. \end{aligned} \quad (8)$$

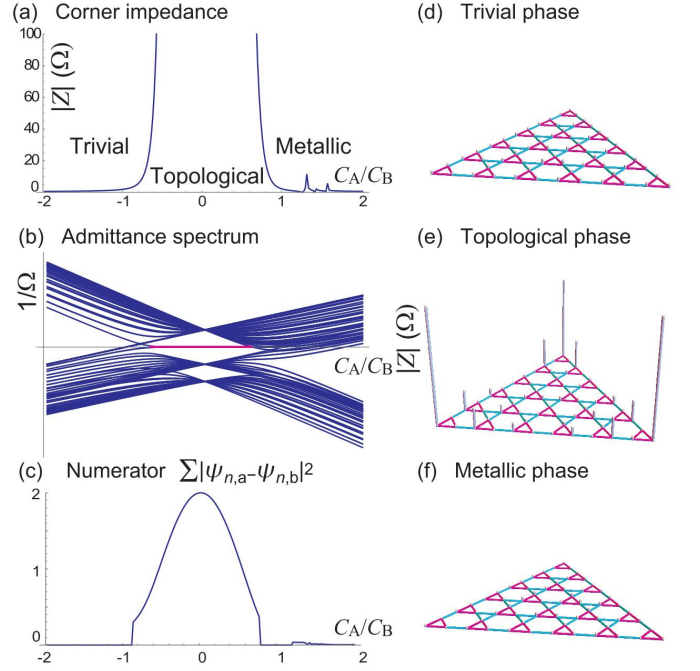


FIG. 2: Two-point impedance for the breathing Kagome circuit. (a) The maximum value of the two-point impedance as a function of C_A/C_B . (b) The admittance spectrum at the resonant frequency $\omega = \omega_c$ as a function of C_A/C_B . (c) The numerator of the impedance $\sum_{n=1}^3 |\psi_{n,a} - \psi_{n,b}|^2$. Spatial distribution of two-point impedance (d) in the trivial phase, (e) in the topological phase, and (f) in the metallic phase. One node is fixed in the vicinity of the triangle center. Absolute value of the impedance is represented by the length of the tubes. We have taken $C_B = 1\mu\text{F}$ and $L = 1\mu\text{H}$. We use a triangle with $\ell = 6$.

Here, C_A and C_B are capacitances shown in Fig.1(a). We note that the Hamiltonian H_{Kagome} is precisely the same one that describes the tight-binding model for the breathing Kagome lattice by replacing C_A and C_B with the hopping parameters t_a and t_b , respectively: See Eq.(1) of Ref.¹⁰. Consequently, the system (7) for the breathing Kagome circuit is topological for $-1 < C_A/C_B < 1/2$, trivial for $C_A/C_B < -1$ and metallic for $C_A/C_B > 1/2$. Consequently, the system undergoes topological phase transitions at $C_A/C_B = -1$ between the trivial and topological phases, and at $C_A/C_B = 1/2$ between the topological and metallic phases. In contrast to the case of CMP, it will be rather easy to make experimental observation of these phase transitions by tuning the capacitance continuously. We note that negative capacitance is possible²¹ with the use of inductors by identifying $C \equiv -1/\omega^2 L$.

We investigate the topological phase in triangular geometry [Fig.1(a)], where topological zero-admittance modes are present at the corners. Due to the presence of zero-admittance modes, the second term in the right-hand side of Eq.(6) vanishes. The resultant equation is a standard formula for the LC circuit with capacitance $C_A + C_B$. The resonant frequency is given by the zero of the identity matrix and given by $\omega_c = 1/\sqrt{2L(C_A + C_B)}$.

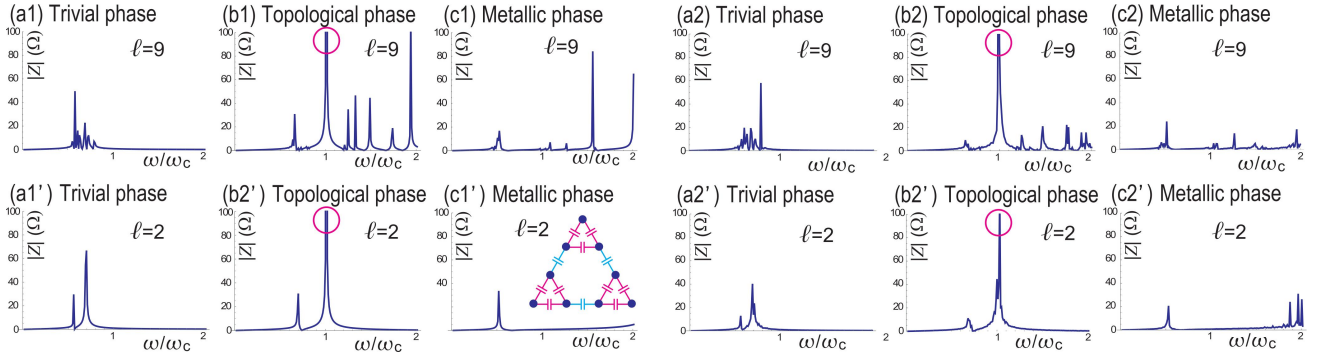


FIG. 3: Corner impedance $|Z|$ as a function of ω/ω_c of the triangle made of the breathing Kagome circuit (a) in the trivial phase ($C_A/C_B = -1.5$), (b) in the topological phase ($C_A/C_B = 0.1$) and (c) in the metallic phase ($C_A/C_B = 1.5$). Red circles indicate the resonance peak arising from topological corner modes. The height of the peak is as huge as $10^9 \Omega$ in the case of $\ell = 9$. The size ℓ is shown in the figure. (a1)–(c1') Corner impedance $|Z|$ without randomness; (a2)–(c2') Corresponding impedance $|Z|$ in the presence of 5% randomness. The inset of (c1') illustrates the breathing Kagome circuit with the size $\ell = 2$.

The behavior of the impedance around ω_c is expressed as

$$|Z| \propto 1/(\omega^2 - \omega_c^2), \quad (9)$$

which yields a huge resonance peak at the frequency ω_c . There is no divergence because of the finite-size effect. On the other hand, when there are no zero-admittance modes, the impedance is finite. The metallic phase is intriguing due to the presence of the sea of zero-admittance modes. As we shall see soon, there is no resonance enhancement in $|Z|$. We expect that the emergence of the resonant modes is a signal that the electric circuit is in a topological phase.

When we use the capacitor of the order of $1\mu\text{F}$ and the inductor of the order $1\mu\text{H}$, the resonance occurs around 1MHz and the impedance is of the order of 1Ω , while the resonant impedance becomes to the order of $10^9\Omega$.

Corner impedance: We consider a triangle structure made of the breathing Kagome circuit [Fig.1]. We first show the admittance spectrum in Fig.2(b), where zero-admittance corner modes emerge only in the topological phase.

We next investigate the two-point impedance. We fix one node a arbitrarily, and measure the impedance Z_{ab} between node a and another node b . By moving b over all nodes, we obtain a space distribution of the two-point impedance. We show the results in the three phases in Fig.2(d)–(f), where node a is taken around the center of the triangle. The essential feature is a strong enhancement of the two-point impedance in the topological phase when node b is taken at three corners. We have found that this essential feature does not depend on the position of the fixed node a provided it is not taken on the corners. When node a is taken on a corner, the strong enhancement appears only when node b is taken at the other two corners because $Z_{aa} = 0$. The huge peak in Z_{ab} is easily understood in the topological phase due to zero-admittance corner modes as we have discussed below Eq.(9). We find that the strongest resonance occurs when two nodes a and b are taken at two different corners.

We show the two-point impedance in Fig.3, where the two nodes are fixed at two different corners. We show the impedance as a function of ω/ω_c . The impedance displays

a huge peak at $\omega = \omega_c$ in the topological phase, while there are no such peaks in the trivial phase and the metallic phase. We also show the impedance at the resonant frequency ω_c as a function of C_A/C_B in Fig.2(a). It becomes huge rapidly in the topological phase, which implies that it is a good indicator to observe topological phases. Remarkably, the resonance peak signaling the topological phase is clearly present in such a small triangle that has the size $\ell = 2$: See Fig.3(a')–(c').

Naively, we expect that the impedance takes a large value also for metallic phase since there are many zero-admittance modes although they are not topological. However, this is not the case. We show the numerator $|\psi_{n,a} - \psi_{n,b}|^2$ as a function of C_A/C_B , where the sum of n is taken only for the three zero-admittance modes in Fig.2(c). It takes value around 2 only for the topological phase representing the two localization of the corner modes. On the other hand, in the metallic phase, it is very small, $|\psi_{n,a} - \psi_{n,b}|^2 \propto 1/N$, where N is the number of nodes. Accordingly, the impedance is small in the metallic phase although there are plenty of zero-admittance modes.

Effects of randomness: We next study the effects of randomness in capacitors and inductors. For this purpose, we make substitution $C_i \mapsto C_i(1 + \eta_i)$ and $L_i \mapsto L_i(1 + \xi_i)$, where η_i and ξ_i are uniformly distributed random variables ranging from $-\delta$ to δ . We have calculated the impedance by choosing $\delta = 0.05$.

We show the ω dependence of the impedance in Fig.3. The prominent peak signaling the topological resonance remains as it is. On the other hand, all other peaks are reduced. The results indicate the topological robustness of the topological corner resonance.

Breathing pyrochlore circuit: A natural extension of the breathing Kagome circuit to three dimensions is the breathing pyrochlore circuit, where a third-order topological insulator is realized¹⁰. The circuit Laplacian is given by

$$L = i\omega \left[3(C_A + C_B) - \frac{1}{\omega^2 L} \right] \mathbb{I} - i\omega H_{\text{pyro}}, \quad (10)$$

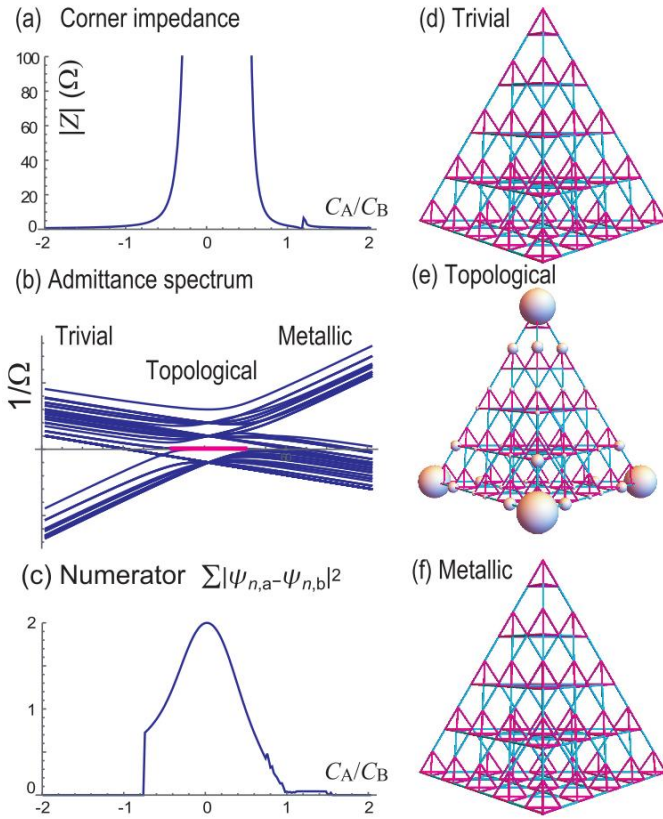


FIG. 4: Two-point impedance for the breathing pyrochlore circuit. (a) The maximum value of the two-point impedance as a function of C_A/C_B . (b) The admittance structure at the resonant frequency $\omega = \omega_c$ as a function of C_A/C_B . (c) The numerator of the impedance $\sum_{n=1}^4 |\psi_{n,a} - \psi_{n,b}|^2$. Spatial distribution of two-point impedance (d) in the trivial phase, (e) in the topological phase, and (f) in the metallic phase. One node is fixed in the vicinity of the tetrahedron center. Absolute value of the impedance is represented by the size of a ball. Huge balls are found at four corners in the topological phase. We have taken $C_B = 1\mu\text{F}$ and $L = 1\mu\text{H}$.

where

$$H_{\text{pyro}} = \begin{pmatrix} 0 & h_{12} & h_{13} & h_{14} \\ h_{12}^* & 0 & h_{23} & h_{24} \\ h_{13}^* & h_{23}^* & 0 & h_{34} \\ h_{14}^* & h_{24}^* & h_{34}^* & 0 \end{pmatrix}, \quad (11)$$

with

$$\begin{aligned} h_{12} &= C_A + C_B e^{-i(k_x+k_y)/2}, \\ h_{13} &= C_A + C_B e^{-i(k_y+k_z)/2}, \\ h_{14} &= C_A + C_B e^{-i(k_z+k_x)/2}, \\ h_{23} &= C_A + C_B e^{-i(k_z-k_x)/2}, \\ h_{24} &= C_A + C_B e^{-i(-k_y+k_z)/2}, \\ h_{34} &= C_A + C_B e^{-i(k_x-k_y)/2}. \end{aligned} \quad (12)$$

The resonant frequency is $\omega_c = 1/\sqrt{3L(C_A + C_B)}$. Topological phase diagram of the breathing pyrochlore circuit is the same as that of the breathing Kagome circuit. We show the admittance spectrum of the tetrahedron in Fig.4(b), where the four topological corner modes appear in the topological phase. We show the two-point impedance between two nodes as a function of C_A/C_B in Fig.4(a), which becomes huge in the topological phase. We also show the numerator $|\psi_{n,a} - \psi_{n,b}|^2$, where the sum of n is taken only for the four zero-admittance modes in Fig.4(c). A space distribution of the two-point impedance is shown in the three phases in Fig.4(d)–(f).

Discussion: We have shown that the topological corner impedance is a good signal to detect a topological phase transition in electric circuits corresponding to the breathing Kagome and pyrochlore lattices, where the huge resonance peak emerges only in the topological phase. The topological phase transition is controlled by tuning variable capacitors. It is not necessary to tune the capacitance so precisely because of the topological robustness. Furthermore, to realize the topological phase together with topological phase transitions, the size of the electric circuit can be quite small.

The author is very much grateful to N. Nagaosa for helpful discussions on the subject. This work is supported by the Grants-in-Aid for Scientific Research from MEXT KAKENHI (Grants No. JP17K05490, No. JP15H05854 and No. JP18H03676). This work is also supported by CREST, JST (JPMJCR16F1).

¹ F. Zhang, C.L. Kane and E.J. Mele, Phys. Rev. Lett. **110**, 046404 (2013).
² W. A. Benalcazar, B. A. Bernevig, and T. L. Hughes, 10.1126/science.aah6442.
³ F. Schindler, A. Cook, M. G. Vergniory, and T. Neupert, in APS March Meeting (2017).
⁴ Y. Peng, Y. Bao, and F. von Oppen, Phys. Rev. B **95**, 235143 (2017).
⁵ J. Langbehn, Y. Peng, L. Trifunovic, F. von Oppen, and P. W. Brouwer, Phys. Rev. Lett. **119**, 246401 (2017).
⁶ Z. Song, Z. Fang, and C. Fang, Phys. Rev. Lett. **119**, 246402 (2017).

⁷ W. A. Benalcazar, B. A. Bernevig, and T. L. Hughes, Phys. Rev. B **96**, 245115 (2017).
⁸ F. Schindler, A. M. Cook, M. G. Vergniory, Z. Wang, S. S. P. Parkin, B. A. Bernevig, and T. Neupert, Science Advances **4**, eaat0346 (2018).
⁹ C. Fang, L. Fu, arXiv:1709.01929.
¹⁰ M. Ezawa, Phys. Rev. Lett. **120**, 026801 (2018).
¹¹ E. Khalaf, H. C. Po, A. Vishwanath and H. Watanabe, Phys. Rev. X **8**, 031070 (2018).
¹² M. Ezawa, Phys. Rev. Lett. **121**, 116801 (2018).
¹³ F. Schindler, Z. Wang, M. G. Vergniory, A. M. Cook, A. Murani, S. Sengupta, A. Y. Kasumov, R. Deblock, S. Jeon, I. Drozdov, H.

- Bouchiat, S. Gueron, A. Yazdani, B. A. Bernevig, and T. Neupert, arXiv:1802.02585.
- ¹⁴ M. Ezawa, Phys. Rev. B 98, 045125 (2018).
- ¹⁵ Z. Wang, B. J. Wieder, J. Li, B. Yan, and B. A. Bernevig, arXiv:1806.11116.
- ¹⁶ M. S.-Garcia, V. Peri, R. Susstrunk, O. R. Bilal, T. Larsen, L. G. Villanueva, S. D. Huber, Nature 555, 342 (2018).
- ¹⁷ H. Xue, Y. Yang, F. Gao, Y. Chong and B. Zhang, cond-mat/arXiv:1806.09418.
- ¹⁸ X. Ni, M. Weiner, A. Alu, and A. B. Khanikaev, cond-mat/arXiv:1807.00896.
- ¹⁹ C. W. Peterson, W. A. Benalcazar, T. L. Hughes and G. Bahl, Nature 555, 346 (2018).
- ²⁰ B. Y. Xie, H. F. Wang, H.-X. Wang, X. Y. Zhu, J.-H. Jiang, M. H. Lu, Y. F. Chen, cond-mat/arXiv:1805.07555.
- ²¹ S. Imhof, C. Berger, F. Bayer, J. Brehm, L. Molenkamp, T. Kiessling, F. Schindler, C. H. Lee, M. Greiter, T. Neupert, R. Thomale, Nat. Phys. 14, 925 (2018).
- ²² M. S.-Garcia, R. Susstrunk and S. D. Huber, cond-mat/arXiv:1806.07367.
- ²³ C. H. Lee, S. Imhof, C. Berger, F. Bayer, J. Brehm, L. W. Molenkamp, T. Kiessling and R. Thomale, Communications Physics, 1, 39 (2018).
- ²⁴ T. Helbig, T. Hofmann, C. H. Lee, R. Thomale, S. Imhof, L. W. Molenkamp and T. Kiessling, cond-mat/arXiv:1807.09555.
- ²⁵ Y. Lu, N. Jia, L. Su, C. Owens, G. Juzeliunas, D. I. Schuster and J. Simon, cond-mat/arXiv:1807.05243.